

Can decaying modes save void models for acceleration?

James P. Zibin*

Department of Physics and Astronomy, University of British Columbia, Vancouver, BC, V6T 1Z1 Canada

(Dated: March 24, 2022)

The unexpected dimness of Type Ia supernovae (SNe), apparently due to accelerated expansion driven by some form of dark energy or modified gravity, has led to attempts to explain the observations using only general relativity with baryonic and cold dark matter, but by dropping the standard assumption of homogeneity on Hubble scales. In particular, the SN data can be explained if we live near the centre of a Hubble-scale void. However, such void models have been shown to be inconsistent with various observations, assuming the void consists of a pure *growing* mode. Here it is shown that models with significant decaying mode contribution today can be ruled out on the basis of the expected cosmic microwave background spectral distortion. This essentially closes one of the very few remaining loopholes in attempts to rule out void models, and strengthens the evidence for Hubble-scale homogeneity.

PACS numbers: 95.36.+x, 98.65.Dx, 98.80.Es, 98.80.Jk

I. INTRODUCTION

In recent years there has been considerable interest in using observations to try to confirm the assumption that the Universe is homogeneous and isotropic on the largest scales. While isotropy about our own worldline follows almost directly from the observed isotropy of the cosmic microwave background (CMB), *radial* homogeneity is difficult to confirm on Hubble scales. Galaxy surveys have found that the distribution of luminous matter to redshifts of at least $z \simeq 0.5$ is largely consistent with the standard cosmological constant plus cold dark matter (Λ CDM) model (e.g., see [1]). However, radial inhomogeneity on the largest scales could be difficult to disentangle from redshift-dependent effects such as evolution, so it is not clear how much current surveys actually tell us about these scales.

Given the isotropy of the CMB, the possibility of radial inhomogeneity might appear very contrived: it would imply that we are near the centre of a (nearly) spherically symmetric Universe, hence apparently violating the Copernican principle. However, just such a situation has received much attention recently, in the context of late-time acceleration. It was realized some years ago [2–4] that if we are situated in an extremely large spherically symmetric underdensity, or void, the luminosity distance-redshift relation of Type Ia supernovae could be explained *without* the need for a cosmological constant or dark energy, or a modification of gravity. (An earlier study of the potential pitfalls of living in a spherical underdensity while assuming a homogeneous model can be found in [5].) These models exchange the coincidence problem of Λ CDM for a violation of the Copernican principle (although they are not free of temporal tuning problems [6], nor do they address the “old” cosmological constant problem). For a recent review of these void

models and the various constraints on them, see, e.g., [7].

General geometrical tests of large-scale homogeneity have been proposed (e.g., see [8, 9]). In the context of void models for acceleration, the strongest and most robust results come from the requirement of fitting the *full* power spectrum of CMB temperature anisotropies. It has been shown that *growing* mode void models which do fit the CMB predict a local Hubble rate far lower than observations indicate [10–14]. Claims have been made [15] that early radiation inhomogeneity can provide a loophole to this conclusion, although this appears unlikely due to the free streaming and rapid redshifting of the radiation [11]. Modifying the primordial perturbation spectrum *might* provide a loophole [10, 16], although order-unity departures from scale invariance, and substantial fine tuning, would be required [11].

Particularly promising tests of homogeneity are those that rely on the scattering of light from inside our past light cone. Void models generically predict large CMB dipoles for off-centre comoving observers [5], and hence should generate anisotropies via the kinetic Sunyaev-Zel’dovich (kSZ) effect [17] (as first suggested in [18]). In Refs. [19, 20], this effect was used to put constraints on void models using galaxy cluster observations, and in [21] the *linear* kSZ effect due to all structure was found to essentially rule out a large class of void models. In [22], it was shown that strong linear kSZ constraints on (growing-mode) void models persisted under a fully relativistic treatment of the problem using the Lemaitre-Tolman-Bondi (LTB) spacetime [23–25]. However, it was stressed in [22] that there were many caveats to the linear kSZ calculations, both technical and relating to the poor state of *model-independent* knowledge of the local baryon fraction and free electron density power.

Another method, which is much less susceptible to the uncertainties which plague the kSZ approach, involves observations of the CMB *spectral* distortions due to Compton scattering from inside the light cone [18]. While the kSZ approach relies on the knowledge of the free electron perturbation power, the calculation of the Compton

*Electronic address: zibin@phas.ubc.ca

y distortion requires only *background* information. Although tight constraints on growing-mode void models using the Compton y distortion have been presented [26], more recent studies using a fully consistent LTB approach have found only very weak constraints [11, 22].

Even though the kSZ effect and spectral distortions both probe the inside of our past light cone, they have so far only been used to gauge possible inhomogeneity *on the surface* of the light cone, at relatively late times. This is because of the usual restriction to *growing* modes of the LTB solution. Both growing and decaying modes are possible [27], but decaying modes are usually discarded on the basis that they imply extreme inhomogeneity at early times, and hence appear difficult to reconcile with standard inflationary scenarios [28]. The assumption of vanishing decaying modes also enables tests based on structure [10, 11, 28], since the growing-mode void can itself be treated as a linear perturbation from a Friedmann-Lemaître-Robertson-Walker (FLRW) spacetime at early times. The absence of decaying modes means that the large dipoles in the LTB models usually studied are mainly *local* to the scatterers—they can be considered as the result of “peculiar velocities” with respect to the CMB frame—and hence the ability of these techniques to probe the inside of the light cone has not been fully exploited.

In standard cosmological models, any decaying modes are assumed to have negligible amplitudes by the end of inflation. Decaying modes on our last scattering surface (LSS) have been observationally constrained to be a subdominant component [29] (see also Ref. [30] for an estimate of the effect of small-amplitude decaying modes on the LSS). In the context of void models for acceleration, however, a decaying mode may be localized around the observer (near the centre of spherical symmetry) and hence not extend to the LSS. Nevertheless, such a decaying mode *would* be visible to a scatterer at the appropriate redshift, and so should be expected to generate substantial spectral distortions and kSZ anisotropies.

It would be ideal to rule out decaying modes in void models on the basis of observations, rather than theoretical prejudices. In addition, it has been suggested that the extra freedom from incorporating a significant decaying mode contribution today might ease the present severe constraints on void models [30, 31]. Therefore, in this work, full use of the power of the y distortion to probe inside the light cone is made to study the observational implications of decaying modes and hence to constrain inhomogeneity at the earliest times. The y distortion is studied rather than the kSZ effect because of the above-mentioned ambiguities with the kSZ approach. The simpler y distortion calculations, combined with the current observational upper limits, will, nevertheless, be sufficient to rule out any contribution of decaying modes significant today, for all but extremely narrow decaying mode profiles.

In Sec. II, the LTB model is introduced and various properties of decaying modes discussed. Next, in

Sec. III, calculation procedures for the y distortion are introduced, both at nonlinear order and under the linear approximation. Results are presented in Sec. IV, before conclusions are made in Sec. V. A covariant derivation of the LTB null geodesic equations is presented in the Appendix. Units are chosen such that $c = 1$.

II. LTB DECAYING MODES

A. General LTB solution

As mentioned in the Introduction, the general LTB spacetime consists of both a growing and a decaying mode [27]. This section begins with a review of the isolation of these modes (based on Ref. [28]), followed by a description of some technical properties of the decaying modes.

For a spherically symmetric distribution of pressureless matter, Einstein’s equations can be solved exactly, resulting in the LTB solution. The metric can be written

$$ds^2 = -dt^2 + \frac{Y'^2}{1-K} dr^2 + Y^2 d\Omega^2, \quad (1)$$

where a prime denotes the derivative with respect to comoving radial coordinate r , and t is the proper time along the comoving worldlines. The function $K = K(r) < 1$ is arbitrary, and the areal radius $Y = Y(t, r)$ is given parametrically by

$$Y = \begin{cases} \frac{M}{K}(1 - \cosh \eta) & K < 0, \\ \frac{M}{K}(1 - \cos \eta) & 0 < K < 1, \\ \left(\frac{9M}{2}\right)^{1/3} (t - t_B)^{2/3} & K = 0, \end{cases} \quad (2)$$

$$t - t_B = \begin{cases} \frac{M}{(-K)^{3/2}}(\sinh \eta - \eta) & K < 0, \\ \frac{M}{K^{3/2}}(\eta - \sin \eta) & 0 < K < 1. \end{cases} \quad (3)$$

Here $M(r)$ is a free radial function, which is set to $M(r) = r^3$ as a gauge condition (this implies that we cannot extend the solution past the “equator” of a closed LTB model).

Various physical quantities can be expressed in terms of these functions (see, e.g., [28]). In particular,

$$4\pi G\rho = \frac{M'}{Y^2 Y'}, \quad (4)$$

$$\theta = H_{\parallel} + 2H_{\perp}, \quad (5)$$

$$\Sigma = \frac{2}{3}(H_{\parallel} - H_{\perp}), \quad (6)$$

$${}^{(3)}R = \frac{2(KY)'}{Y^2 Y'}, \quad (7)$$

where ρ , θ , and Σ are the matter density, expansion, and shear scalar, respectively, for the comoving worldlines. For comoving shear tensor $\sigma_{\mu\nu}$ and radial spatial unit vector r^μ ($r^\mu u_\mu = 0$), we have $\Sigma = \sigma_{\mu\nu} r^\mu r^\nu$. ${}^{(3)}R$ is the Ricci curvature of the spatial comoving-orthogonal hypersurfaces. The radial and transverse expansion rates are given, respectively, by

$$H_{\parallel} = \frac{\dot{Y}'}{Y'}, \quad H_{\perp} = \frac{\dot{Y}}{Y}, \quad (8)$$

where the overdot denotes the derivative with respect to t .

This exact solution contains another free radial function, $t_B = t_B(r)$, which is known as the ‘‘bang time’’ function since $t = t_B(r)$ implies $Y = 0$, leading to divergences in each of ρ , θ , and ${}^{(3)}R$. In the models of interest here, this will correspond to the cosmological singularity. When $t_B(r)$ is not constant, it is often stated that the big bang occurs at different times at different locations. However, we are of course free to define a new time coordinate \tilde{t} such that the big bang occurs ‘‘simultaneously’’ at $\tilde{t} = 0$. The *physical* content of a varying t_B is related to the divergence of covariant quantities such as the shear scalar, Σ , as $t \rightarrow t_B$.

As described in [28], small-amplitude variations in spatial curvature, ${}^{(3)}R$, correspond to growing-mode perturbations about an Einstein-de Sitter (EdS) FLRW model, while appropriately small variations in bang time correspond to decaying modes. Therefore, according to Eq. (7), to isolate a pure decaying mode we must set $K(r) = 0$. The LTB solution, Eqs. (2) and (3), then becomes

$$Y = \left(\frac{9M}{2}\right)^{1/3} (t - t_B)^{2/3}. \quad (9)$$

In the remainder of this work, only pure decaying modes will be considered. Justification for this will be discussed in Sec. V. The main motivation of this study is to examine the effect of decaying modes that are significant today. In Sec. III C we will see that this implies that we are interested in bang time fluctuations $\delta t_B(r) \sim t_0$, where t_0 is the proper age today.

B. Properties of decaying modes

Since significant decaying modes are not normally expected in standard inflationary scenarios, it will be worthwhile to explicate some of their counterintuitive properties. Indeed, in the years *before* inflation was proposed, decaying modes were studied extensively, as there was no reason to ignore them *a priori*. In particular, under the guise of ‘‘delayed cores’’ of the big bang, they were proposed as an explanation for quasars [32]. LTB decaying modes are generalizations of Schwarzschild white holes, which are time-reversed analogs of black holes.

An important property of LTB models involves the presence of *shell crossings*, where comoving worldlines intersect and hence the pressure-free assumption becomes invalid. In [33], criteria were derived to ensure that no shell crossings occur; for the case of our $K(r) = 0$ pure decaying mode spacetime, they become

$$t'_B \leq 0. \quad (10)$$

This condition restricts us to situations in which the big bang singularity is ‘‘delayed’’ at the origin, i.e. $t_B(r = 0) \geq t_B(r)$. Throughout this work, the condition (10) will be assumed to hold.

Another relevant feature of LTB decaying modes is the generic presence of cosmological *blueshifts*, and possibly *divergent blueshifts*. In [34] it was shown that light rays emitted near the initial singularity will generically be blueshifted at late times when $t'_B \neq 0$. This might mean, e.g., that an observer whose LSS intersected a decaying mode would observe the CMB temperature in the direction of the decaying mode to be *greater* than the actual recombination temperature! In addition, in [35] it was pointed out that under certain circumstances, divergent blueshifts can arise in such models, with the result that the white hole will be unstable and will convert into a black hole. This blueshift behaviour can be understood broadly by noting that for $t'_B \neq 0$, the spacetime becomes shear dominated at early times. Since the shear is defined to be trace free, this means that in some directions the comoving worldlines will be *contracting* near the singularity. In particular, the *radial* expansion rate H_{\parallel} will be negative close enough to the singularity, leading to blueshifts for null rays that are approximately radial. (A related discussion appears in Ref. [36].)

In the void model context, a decaying mode near the centre would not be directly observable by a central observer. However, a scatterer at the appropriate redshift down the central observer’s light cone *would* see the blueshifts due to the decaying mode, and hence would observe a strongly anisotropic CMB sky. This suggests that the scatterer would produce significant CMB spectral distortions (or kSZ anisotropies). Of course in a realistic cosmology, the dust source approximation of LTB breaks down at early times, when radiation becomes important. It is not clear how the blueshift behaviour will be modified in the radiation era. However, since recombination occurs somewhat after radiation domination, the large blueshifts will be incurred during the dust era, when the LTB solution is reliable. Thus the constraints from the spectral distortion will be sound.

III. CALCULATING THE SPECTRAL y DISTORTION

A. The y distortion

The y distortion arises from the Compton scattering of anisotropic CMB radiation from inside our past light

cone into our line of sight. In the single-scattering approximation, and in a spherically symmetric spacetime, it can be written as [37]

$$y = \frac{3}{16} \int_0^{z_{\text{re}}} dz_s \frac{d\tau}{dz_s} \int_0^\pi d\xi \sin \xi (1 + \cos^2 \xi) \ln^2 \left(\frac{T(z_s, \xi)}{T(z_s, \pi)} \right). \quad (11)$$

Here τ is the optical depth, and the outer integral only extends to the redshift of (the assumed abrupt) reionization, z_{re} . $T(z_s, \xi)$ is the CMB temperature seen by a scatterer at redshift z_s from the central observer. Spherical symmetry implies that the temperature is a function of only one angle, ξ . A radially outwards directed ray is chosen to have $\xi = 0$. Although in standard models we have $z_{\text{re}} \simeq 10$, the reionization redshift could be somewhat different in void models. Nevertheless, in the models studied here, most of the contribution to the redshift integral will come from $z_s \simeq 3$, so uncertainty in z_{re} should not affect the final results significantly. The factor $d\tau/dz_s$ can be readily written in terms of the background quantities as [22]

$$\frac{d\tau}{dz_s} = \frac{\sigma_T f_b (2 - Y_{\text{He}}) \rho_m(z_s)}{2m_p(1 + z_s)H_{\parallel}(z_s)}. \quad (12)$$

Here σ_T is the Thomson cross section, $f_b \equiv \rho_b/\rho_m$ is the baryonic to total matter fraction, Y_{He} is the helium mass fraction, and m_p is the proton mass.

In the case that the fluctuations over the sky in $T(z_s, \xi)$ are small, and dominated by the dipole $\beta(z_s)$, Eq. (11) becomes [11]

$$y = \frac{7}{10} \int_0^{z_{\text{re}}} dz_s \frac{d\tau}{dz_s} \beta(z_s)^2. \quad (13)$$

We will see that this is generally not a good approximation for decaying mode void models.

The best current constraints on the y distortion come from the COsmic Background Explorer (COBE) satellite, which found $y < 1.5 \times 10^{-5}$ at 2σ confidence [38].

B. Nonlinear calculation of CMB anisotropies

In order to evaluate the y distortion expression, Eq. (11), we need to know the CMB temperature anisotropy seen by a scatterer at redshift z_s , $T(z_s, \xi)$. To evaluate this temperature, we need to determine the redshifts along various (generally nonradial) null geodesics. The general exact expression for redshift (e.g., see [39]), applied to a geodesic comoving congruence of worldlines, gives

$$1 + z(t, \xi) = \exp \left[\int_t^{t_e} \left(\frac{1}{3} \theta + \sigma_{\mu\nu} n^\mu n^\nu \right) dt \right]. \quad (14)$$

Here $z(t, \xi)$ is the total redshift incurred along the null geodesic between an arbitrary point, at proper time t ,

and the ray's endpoint, at $t = t_e$. The integral is evaluated along the null ray. The vector $n^\mu(t)$ is the normalized projection of the geodesic's tangent vector, v^μ , orthogonal to the comoving timelike vector field u^μ (see the Appendix). In other words, $n^\mu(t)$ is the spatial direction of propagation of the null ray seen by a comoving observer. At the endpoint of the geodesic, $n^\mu(t_e)$ is directed at angle ξ with respect to the radially outwards direction, i.e. $r_\mu n^\mu(t_e) = \cos \xi$.

In order to evaluate Eq. (14), we must first know how to determine the past-directed null geodesic with initial condition (IC) ξ or $n^\mu(t_e)$, and then we must know where to stop evolving the geodesic, i.e. we must know how to find the LSS. The first problem is straightforward, in that we must solve the null geodesic equation

$$v^\mu_{;\nu} v^\nu = 0. \quad (15)$$

Extracting various components of Eq. (15) (see the Appendix) gives

$$\frac{dt}{d\lambda} = \gamma, \quad (16)$$

$$\frac{dr}{d\lambda} = \frac{\gamma n_r}{Y'}, \quad (17)$$

$$\frac{d\theta}{d\lambda} = \frac{L}{Y^2}, \quad (18)$$

$$\frac{dn_r}{d\lambda} = \frac{1}{2} \gamma (n_r^2 - 1) \left(3\Sigma n_r - \frac{2}{Y} \right). \quad (19)$$

Here θ is the standard spherical angular (comoving) coordinate of the photon (the second spherical angle can be chosen to be constant), λ is an affine parameter along the null ray, γ is defined by Eq. (16), $n_r \equiv n^\mu r_\mu$, and L is a constant. Finally, Eq. (14) now gives

$$1 + z(t, \xi) = \frac{\gamma}{\gamma_e}. \quad (20)$$

The set of coupled ordinary differential equations (16) to (19), together with the ICs (i.e. the endpoint values) t_e , r_e , $\theta_e \equiv 0$, $n_{r,e} = \cos \xi$, and γ_e , can then be solved numerically with standard techniques.

Finding the LSS, i.e. knowing where to stop the geodesic integration, necessarily involves some assumptions, since the details of recombination in the region of the decaying mode are unclear. In this work, it will be assumed that recombination occurs at the same energy density and local temperature within the decaying mode as asymptotically outside. Schematically, the approach is to first use Eqs. (16) to (20) to evolve a null geodesic from the centre of symmetry today into the past to a redshift of $z_{\text{LS}} = 1091$, where the energy density ρ_{LS} is evaluated. Then, for each scatterer redshift z_s , several null rays are propagated, again into the past, from the scatterer in several spatial directions as characterized by the initial angle ξ . These null rays are evolved until the local energy density reaches ρ_{LS} , at time $t_{\text{LS}}(\xi)$, which is taken to define the LSS in that direction. The total

redshift, $z(t_{\text{LS}}(\xi), \xi)$, incurred from the central point today, to the scatterer, to the LSS, is then evaluated using Eq. (20). Finally, the temperature observed at the scatterer in direction ξ can be written

$$T(z_s, \xi) = T_0 \frac{(1 + z_{\text{LS}})(1 + z_s)}{1 + z(t_{\text{LS}}(\xi), \xi)}, \quad (21)$$

where T_0 is the (unscattered) CMB temperature today. This expression can then be used to evaluate the integral for the y distortion, Eq. (11). Note that this technique generalizes that of Ref. [11] to the case of nonradial geodesics, and to a LSS determined by fixed density, rather than fixed proper time (which is a reasonable approximation in the case of vanishing decaying modes). The dipole $\beta(z_s)$ in Eq. (13) is calculated in the LTB model by propagating past-directed null rays radially inwards and outwards from the scatterer to ρ_{LS} , and comparing the resulting redshifts as described in [11].

Importantly, the uncertainties about recombination in the decaying mode region will likely affect the calculations of $T(z_s, \xi)$ and hence of y . Since the temperature at recombination is determined by *local* atomic physics, the assumption that the recombination temperature is constant is likely reasonable. However, it is certainly possible that there may be order-unity uncertainties in the density at recombination, due to the presence of shear close to the singularity. (Likewise, as mentioned earlier, the radiation component absent from the LTB solution is expected to affect the $T(z_s, \xi)$ calculation at the level of tens of percent.) Nevertheless, we will see that the results presented here are powerful enough that order-unity variations in the density will not affect the final conclusions.

C. Linear calculation of CMB anisotropies

As a check of the nonlinear calculation described in Sec. III B, and especially given that such calculations for decaying modes have apparently not been made previously, it will be useful to perform an alternative calculation of $T(z_s, \xi)$ in the case where a linear description is valid. A decaying mode associated with bang time fluctuation $\delta t_B(r)$ will be accurately described by linear theory at time t when $\delta t_B(r)/t \ll 1$ [28]. (This explains the condition $\delta t_B(r) \sim t_0$ for decaying modes to have significant amplitude today.) Therefore, if we satisfy $\delta t_B(r)/t_{\text{LS}} \ll 1$ at the time of recombination, then the spacetime will be accurately described by a linear perturbation from FLRW for all times after recombination (since growing modes are ignored).

In particular, we can describe a small-amplitude decaying mode in terms of linear metric perturbations in some gauge. A convenient choice is Newtonian (or zero shear) gauge, for which the vanishing of anisotropic stress implies that there is only one unique metric perturbation, ψ , which describes both the lapse and isotropic spatial metric (curvature) perturbations (e.g., see [40]). Then

the temperature anisotropy viewed in direction n^μ is described by the Sachs-Wolfe (SW) effect [41]. In the approximation of abrupt recombination (which is a good approximation on large scales), this can be written [39]

$$\frac{\delta T(n^\mu)}{T_e} = 2 \int_{t_{\text{LS}}}^{t_e} \dot{\psi} dt + \frac{1}{3} \psi - \frac{2}{9} \left(\frac{3}{H} \dot{\psi} - \frac{\nabla^2}{a^2 H^2} \psi \right) - \frac{2}{3} \frac{1}{H^2} \left(\dot{\psi} + H\psi \right)_{;\mu} n^\mu. \quad (22)$$

Here a and H are the FLRW background scale factor and Hubble rate, and the quantities outside the integral are to be evaluated at the point on the LSS in direction n^μ . T_e is the background temperature at the null ray endpoint (normally taken to be the scatterer at z_s). (Note that Eq. (22) corrects a typographical sign error in [39].)

Equation (22) is general in that it applies to growing or decaying modes. However, we can simplify it for the case of decaying modes. In a dust background, the metric perturbation ψ satisfies the equation (e.g., see [40])

$$\ddot{\psi} + 4H\dot{\psi} = 0. \quad (23)$$

The decaying mode solution is

$$\psi(t, r) = \psi(t_e, r) \left(\frac{t_e}{t} \right)^{5/3}, \quad (24)$$

which implies

$$\dot{\psi} = -\frac{5}{2} H \psi. \quad (25)$$

Substituting Eq. (25) into Eq. (22) gives

$$\frac{\delta T(n^\mu)}{T_e} = -5 \int_{t_{\text{LS}}}^{t_e} \psi(t, r(t)) H(t) dt + 2\psi + \frac{2}{9} \frac{\nabla^2}{a^2 H^2} \psi + \frac{1}{H} \psi_{;\mu} n^\mu. \quad (26)$$

In an EdS background, the radial component of the null trajectory is given by

$$r(t) = \sqrt{r_e^2 + \Delta r^2 - 2r_e \Delta r \cos \xi}, \quad (27)$$

where

$$\Delta r(t) \equiv \frac{2}{a_e H_e} \left[1 - \left(\frac{t}{t_e} \right)^{1/3} \right]. \quad (28)$$

Equation (26) is the final expression for the decaying mode SW effect. Note, in particular, that it includes an *integrated* SW component, since even in an EdS background, ψ is time dependent.

The final step is to relate the metric perturbation $\psi(r)$ to the bang time fluctuation, $t_B(r)$. To do this, first note that the relation

$$\frac{\delta \rho}{\rho} = \frac{2}{3} \frac{\nabla^2}{a^2 H^2} \psi, \quad (29)$$

where $\delta\rho$ is the *comoving* density perturbation, holds for both growing and decaying modes. Then, expanding Eq. (4) with Eq. (9) in terms of the small parameter $t_B(r)/t$, we can write

$$\frac{\delta\rho}{\rho} = 2 \left(\frac{t_B}{t} + \frac{t'_B}{t} \frac{M}{M'} \right) + \mathcal{O} \left(\frac{t_B}{t} \right)^2. \quad (30)$$

Note that this result generalizes the corresponding result in [28] to the case of significant bang time gradients, t'_B . Now, given a bang time function, all the pieces are in place to perform the linearized calculation of the CMB anisotropies, and hence of the y distortion.

IV. RESULTS

A. Bang time profile

In order to calculate the y distortion, we must first choose a bang time function. A convenient choice is a Gaussian profile, specified by

$$t_B(r) = t_{B,m} e^{-r^2/L^2}, \quad (31)$$

with amplitude $t_{B,m} > 0$ and characteristic width L . This specification is all we need to calculate the y distortion according to the nonlinear prescription of Sec. III B. However, for the linear calculation of Sec. III C, we first need to determine the corresponding metric perturbation, ψ . It is straightforward to show that Eqs. (29) and (30) are satisfied when ψ takes the form

$$\psi(t, r) = - (a_0 L H_0)^2 \frac{t_{B,m}}{2t_0} \left(\frac{t_0}{t} \right)^{5/3} e^{-r^2/L^2}. \quad (32)$$

Here the right-hand side has been written in terms of the quantities today, a_0 , H_0 , and t_0 , since they are constant. The fact that $\psi(t, r)$ is also a spatial Gaussian explains why the Gaussian choice for $t_B(r)$ is convenient.

For the calculations presented in this section, units were chosen such that $100 \text{ km s}^{-1} \text{ Mpc}^{-1} = 1$ and $4\pi G = 1$. This means that realistic values of the Hubble parameter today are $H_0 \simeq 0.7$, and that values of the matter density and proper time today are both of order unity. It is difficult in general inhomogeneous cosmologies to unambiguously describe distances. Therefore, the bang time profile width L will be translated into a corresponding redshift down the central observer's light cone, $z_L \equiv z(r = L)$. As already mentioned, we will be primarily interested in the regime $t_{B,m} \sim t_0$, in which the decaying modes will have a significant effect at late times. All of the calculations in this study used a value $H_0 = 0.7$ and integrated to a reionization redshift of $z_{\text{re}} = 11$.

B. Convergence to linear theory

Before calculating the y distortion, it will be important to check that the nonlinear calculation of temperature

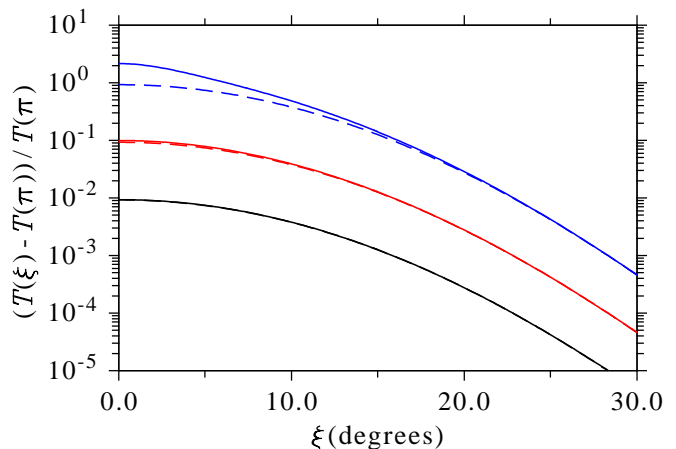


FIG. 1: CMB temperature anisotropy visible to a scatterer at $(t, r) = (1.0, 1.15)$. The angle ξ is measured from the radial direction, i.e. $\xi = 0$ corresponds to the centre of the anisotropy. Each solid curve represents a nonlinear calculation using the method of Sec. III B, while each dashed curve used the linear method of Sec. III C. The bang time amplitude took the values $t_{B,m} = 1.0 \times 10^{-3}$, 1.0×10^{-4} , and 1.0×10^{-5} , for the top (blue) curves, middle (red) curves, and bottom (black) curves, respectively. The nonlinear and linear calculations converge at the smallest bang time amplitudes, as expected (the bottom two curves are almost indistinguishable).

anisotropies agrees with the linear calculation, in the appropriate limit. In Fig. 1, the anisotropy $T(t_s, r_s, \xi)$ is displayed for a scatterer at position $(t_s, r_s) = (1.0, 1.15)$, calculated using both the nonlinear and linear approaches. The scatterer's position is such that the scatterer's past light cone intersects the decaying mode somewhat away from the peak of the Gaussian (although the results are qualitatively similar for *any* scatterer position). The calculations used a profile width of $L = 0.25$, which corresponds to $z_L \simeq 0.35$. As the decaying mode amplitude $t_{B,m}$ decreases, it is apparent that the two calculations converge, as expected. This is particularly reassuring, considering how very different the anisotropy calculations are for linearized EdS and nonlinear LTB. In addition, notice that the anisotropy becomes of order unity already for the relatively small amplitude $t_{B,m} = 1.0 \times 10^{-3}$. For decaying modes of significant amplitude today, i.e. $t_{B,m} \sim t_0 \sim 1$, we therefore expect extreme anisotropies at the scatterers, due to the blueshifts mentioned previously.

For the calculations in Fig. 1, the time of last scattering corresponds to $t_{\text{LS}} = 2.8 \times 10^{-5}$ (in the *linear* regime, in which t_{LS} is independent of position). Therefore, the three pairs of curves in that figure correspond to $t_{B,m}/t_{\text{LS}} = 36.1$, 3.61 , and 0.361 , from top to bottom. We can see that the linear approximation is good even for ratios $t_{B,m}/t_{\text{LS}}$ of order unity. Thus the condition $t_{B,m}/t_{\text{LS}} \ll 1$ given in Sec. III C for the validity of linear theory is too stringent. To understand the reason for this, note that the anisotropies shown in Fig. 1 are small, even

when $t_{B,m}/t_{LS}$ is of order unity. This occurs because of a near cancellation of the first two terms in the decaying mode SW effect, Eq. (26). Therefore, a metric perturbation ψ of order unity can produce small anisotropy, $\delta T/T$. This is in contrast to the familiar *growing* mode case, where the SW anisotropy will be of the same order as ψ . Intuitively, a decaying mode *decays*, and hence has much less effect integrated over the null ray than a growing mode. Note, finally, that this also means that it is important to include the gradient terms in Eq. (26), even for the Hubble-scale decaying modes considered here.

C. y distortion

With all of the tools in place, we can now calculate the y distortion. Figure 2 displays the y distortion as a function of the dimensionless bang time profile amplitude, $t_{B,m}/t_0$. These calculations also used a profile width of $L = 0.25$, which corresponds to $z_L \simeq 0.35$. Curves are shown for the full-sky integration based on Eq. (11), together with the dipole approximation, Eq. (13). Also, anisotropies are calculated using the nonlinear approach of Sec. III B, as well as the linearized SW approach from Sec. III C. It is evident, again, that the nonlinear calculation approaches the linear one for small bang time amplitudes, and that both exhibit the expected quadratic dependence of y on $t_{B,m}/t_0$ in the linear regime. It is clear as well that the dipole approximation substantially overestimates the spectral distortion, especially at the lower amplitudes. Most striking, however, is the fact that the y distortion exceeds the COBE limit by orders of magnitude, for decaying modes which are significant today (i.e. for $t_{B,m}/t_0 \sim 1$), at least for decaying modes with width $z_L \simeq 0.35$.

We should expect that the y distortion will decrease as the decaying mode profile width decreases, due to the smaller solid angle sourcing the angular integral in Eq. (11). Also, the anisotropies themselves should be affected [e.g. via the L^2 factor in Eq. (32)], although it is not clear exactly what L dependence is expected, due to the subtle cancellations that occur in the SW expression, Eq. (26). In Fig. 3, the y distortion is plotted versus decaying mode width, z_L , at fixed bang time amplitude, $t_{B,m}/t_0 = 0.2$. These calculations used the nonlinear approach of Sec. III B. A marked decrease in y as z_L decreases is visible, with y dropping below the COBE limit for $z_L \lesssim 0.02$. Also notable is the fact that the dipole approximation severely underestimates the drop in y . This is understandable, since the dipole approximation misses the solid angle effect mentioned above. Finally, note that, for the profiles able to evade the COBE constraint ($z_L \lesssim 0.02$), the profile width must be very small relative to cosmological scales.

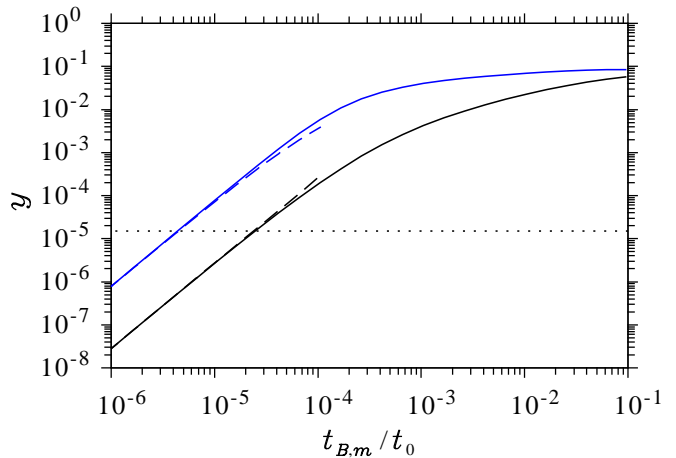


FIG. 2: y distortion versus dimensionless bang time amplitude, $t_{B,m}/t_0$, at fixed profile width $L = 0.25$, which corresponds to $z_L \simeq 0.35$. The black (lower) curves used the full-sky integration, Eq. (11), while the blue (upper) curves used the dipole approximation, Eq. (13). Each solid curve used the nonlinear anisotropy calculation of Sec. III B, and the dashed curves used the linearized SW approach of Sec. III C. The nonlinear and linear calculations converge at the smallest bang time amplitudes, as expected. The dotted line indicates the COBE upper limit of $y < 1.5 \times 10^{-5}$ at 2σ confidence [38].

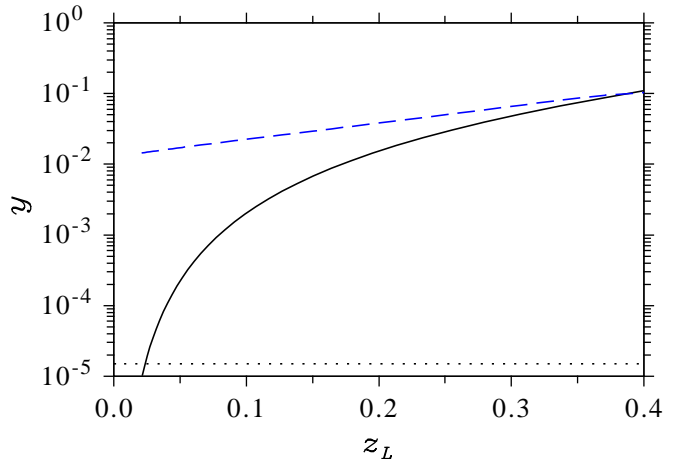


FIG. 3: y distortion versus decaying mode width, z_L , at fixed bang time amplitude, $t_{B,m}/t_0 = 0.2$. The black (solid) curve used the full-sky integration, Eq. (11), while the blue (dashed) curve used the dipole approximation, Eq. (13). The dotted line indicates the COBE upper limit of $y < 1.5 \times 10^{-5}$ at 2σ confidence [38].

V. CONCLUSIONS

As discussed in Sec. II B, cosmological decaying modes suffer from a variety of problems. They should have decayed to negligible amplitudes by the end of inflation, and no mechanism has been proposed for the generation of decaying modes so large as to still be significant

today. They must satisfy the condition $t'_B \leq 0$ to avoid shell crossings, although there is something oddly restrictive about this criterion: clearly a generic profile in the absence (or even in the presence) of spherical symmetry will violate it somewhere. Of course, without an explicit mechanism of formation, not much else can be said. The possibility of blueshift instability would also need to be addressed for these models.

In addition, if we are to save void models for acceleration by adding a significant decaying mode contribution today, then the ICs would need to be exquisitely finely tuned. In the *linear* regime, the metric perturbation ψ is constant in the growing mode, but obeys Eq. (24) for the decaying mode. Therefore the ratio between growing and decaying modes increases like $t^{5/3}$. A ratio of order unity today implies that the growing modes must be suppressed by a factor $(t_{\text{LS}}/t_0)^{5/3} \sim 10^{-8}$ at last scattering. Of course this estimate will be quantitatively affected by the breakdown of linear theory at early times, but the conclusion will still hold qualitatively: In a model with significant decaying modes today, the extremely inhomogeneous early Universe must be pure decaying mode to very high precision.

One further problem with decaying mode models is related to the shear domination at early times. Since the details of big bang nucleosynthesis (BBN) depend on the expansion history of the early Universe, we can expect substantial departures from standard BBN in these models. Since the decaying mode profile must be centred near our own worldline, we would not expect the observed local light-element abundances to agree with predictions based on the standard Λ CDM model.

Nevertheless, in this study decaying modes have been given the “benefit of the doubt,” in that it has been assumed that all of these problems could be somehow overcome, and the observational consequences of decaying modes have been examined. As mentioned in the [Introduction](#), while *growing* mode LTB void models for acceleration have been essentially ruled out on the basis of CMB + H_0 , kSZ, and other observations, it might be possible that a significant contribution today of LTB decaying mode could allow such models to survive those tests. The generic presence of blueshifts near the cosmological singularity of a decaying mode, however, suggests that these inhomogeneous bang time models might be susceptible to probes of the interior of our past light cone. Therefore, a procedure for calculating CMB temperature anisotropies for a scatterer whose LSS crosses a decaying mode was developed and used to calculate the y distortion in these models. Although the results will necessarily be dependent upon the uncertainties regarding recombination inside a decaying mode, the constraints were so strong that even order-unity uncertainties in the calculated anisotropies will have negligible effect on the conclusions. Decaying modes which are significant today and wider than $z_L \simeq 0.02$ are ruled out by the y distortion test. Narrower profiles might survive this test, but would almost certainly suffer from obvious problems

in local surveys: the region inside $z_L \simeq 0.02$ would be *much* younger than the outside, and hence would have a substantially higher density and expansion rate. In addition, structure would presumably have substantially less power on the inside. The local Universe to $z \simeq 0.02$ is well surveyed, and no such discontinuities are apparent.

It is worth stressing that decaying modes with sufficiently small amplitudes, i.e. $t_{B,m}/t_0 \lesssim 10^{-5}$, are not ruled out by the y distortion test. Although such perturbations may suffer some of the problems with decaying modes listed above, it is conceivable that they play a role in cosmology [29]. However, the effects of decaying modes with such small amplitudes will be negligible today, and hence will not ease the severe constraints on growing-mode void models for acceleration.

Note that the philosophy of this study has been to examine the spectral distortions due to *pure* decaying modes. Of course one could argue that a model which evades the CMB + H_0 and kSZ tests might consist of a superposition of decaying and growing modes. However, given that pure growing-mode models typically produce values of the y distortion below the COBE limit [22], it appears very likely that the addition of growing modes of typical amplitudes will not change the conclusions of this study significantly. Of course the combined effect of growing and decaying modes will generally not be a simple linear superposition, due to the nonlinearity of general relativity. But the extremely large anisotropies in decaying mode models are due fundamentally to the extreme inhomogeneity at early times, when a growing-mode contribution will be negligible.

Therefore, it appears that decaying modes do not provide a loophole to the conclusion that void models cannot explain acceleration. This result strengthens our confidence in the standard paradigm of a homogeneous, isotropic, accelerating cosmology, driven by some mysterious form of dark energy or modified gravity.

Acknowledgments

I thank Albert Stebbins and Andrzej Krasiński for useful discussions. This research was supported by the Canadian Space Agency.

Note added.—After this work was essentially complete, a closely related paper appeared [14], which also studied the observational consequences of decaying modes which are significant today. There are a few major differences to our approaches. First, Ref. [14] did not exclude the “advanced” big bang case, $t'_B > 0$. This case was excluded in the present study since the consequent early shell crossings were argued to render the early-time LTB solution, and hence the temperature anisotropy calculations, unreliable. Another difference is that Ref. [14] used the kSZ effect in clusters as the basis of its constraints, as opposed to the y distortion used here. However, Ref. [14] used the dipole approximation for the anisotropies seen

by the scatterers. Finally, the models studied in [14] included LTB growing modes. The strong findings of [14] are in agreement with those of the present study, and hence reinforce the conclusion that models with significant decaying modes today are not viable.

Appendix: Covariant null geodesic equations

1. 1 + 1 + 2 formalism

The nonradial null geodesic equations in the LTB spacetime have been derived many times before (e.g., see [34, 42–44]). In this appendix, a novel derivation is presented which is based on the covariant 1 + 1 + 2 formalism, and, in particular, makes no use of Christoffel symbols.

This subsection will begin with a brief summary of the covariant 1 + 3 formalism. More details can be found in the reviews [45, 46]. This formalism is based upon a fundamental timelike vector field, u^μ (normalized according to $u^\mu u_\mu = -1$), which is conveniently taken to be tangent to the dust comoving worldlines in the LTB spacetime. The tensor

$$h^\mu{}_\nu \equiv \delta^\mu{}_\nu + u^\mu u_\nu \quad (\text{A.1})$$

projects orthogonal to u^μ . We can use $h_{\mu\nu}$ to define a spatial covariant derivative according to

$$D_\mu T_{\nu_1 \nu_2 \dots \nu_n} \equiv h^\lambda{}_\mu h^{\sigma_1}{}_{\nu_1} h^{\sigma_2}{}_{\nu_2} \dots h^{\sigma_n}{}_{\nu_n} T_{\sigma_1 \sigma_2 \dots \sigma_n; \lambda}, \quad (\text{A.2})$$

for any tensor $T_{\nu_1 \nu_2 \dots \nu_n}$ orthogonal to u^μ in all of its indices.

For the case of twist-free dust, which is the case for the LTB model, we can decompose the covariant derivative of u_μ according to

$$u_{\mu; \nu} = \frac{1}{3} \theta h_{\mu\nu} + \sigma_{\mu\nu}. \quad (\text{A.3})$$

The scalar θ measures the local volume rate of expansion of the congruence u^μ . The trace-free, symmetric tensor $\sigma_{\mu\nu}$ measures the local rate of shear of the congruence, and is orthogonal to u^μ in both of its indices. For a dust source, the acceleration of the comoving worldlines vanishes, i.e. $u_{\mu; \rho} u^\rho = 0$.

Under spherical symmetry, each comoving-orthogonal slice contains a preferred spacelike congruence with radial tangent vector r^μ , where $r^\mu r_\mu = 1$. In this case, the 1 + 3 covariant approach can be generalized to the so-called 1 + 1 + 2 approach, which incorporates both u^μ and r^μ as fundamental fields [47–49]. By analogy with the tensor $h^\mu{}_\nu$ defined in Eq. (A.1), which projects into the slices, we can define a tensor $s^\mu{}_\nu$ by

$$s^\mu{}_\nu \equiv h^\mu{}_\nu - r^\mu r_\nu, \quad (\text{A.4})$$

which projects into the two-spheres (called *sheets*) orthogonal to both u^μ and r^μ .

Under spherical symmetry, a spatial three-tensor such as the shear $\sigma_{\mu\nu}$ must be expressible in terms of r^μ , $s^{\mu\nu}$, and a two-scalar Σ . Explicitly, we can write

$$\sigma_{\mu\nu} = \left(r_\mu r_\nu - \frac{1}{2} s_{\mu\nu} \right) \Sigma. \quad (\text{A.5})$$

This implies that the shear scalar can be written $\Sigma = \sigma_{\mu\nu} r^\mu r^\nu$.

2. Null geodesics

The tangent vector v^μ to a null geodesic can be decomposed into components parallel and orthogonal to the dust four-velocity u^μ according to

$$v^\mu = \gamma(u^\mu + n^\mu), \quad (\text{A.6})$$

where the spatial propagation direction n^μ satisfies $n^\mu u_\mu = 0$ and $n^\mu n_\mu = 1$. By virtue of the relation $v^\mu u_\mu = -\gamma$, the photon energy (or blackbody spectrum temperature) is proportional to γ . For any null geodesic in a spherically symmetric background, n^μ will be constrained to a two-dimensional subspace of each comoving slice. In other words, n^μ can be decomposed into components parallel to r^μ and parallel to an angular direction, denoted θ^μ , where $\theta^\mu \theta_\mu = 1$ and $\theta^\mu u_\mu = \theta^\mu r_\mu = 0$. Explicitly,

$$n^\mu = n_r r^\mu + n_\theta \theta^\mu. \quad (\text{A.7})$$

Using Eq. (A.5) we can calculate the following projections of the shear tensor:

$$\sigma_{\mu\nu} r^\mu n^\nu = \Sigma n_r, \quad \sigma_{\mu\nu} n^\mu n^\nu = \frac{1}{2} \Sigma (3n_r^2 - 1). \quad (\text{A.8})$$

The null geodesic equation can be written

$$v^\mu{}_{; \nu} v^\nu = \frac{dv^\mu}{d\lambda} = 0, \quad (\text{A.9})$$

where λ is an affine parameter along the geodesic. Our goal will be to evaluate the various components of the geodesic equation. For the time component, using Eqs. (A.3) and (A.8) we find

$$\frac{d(v^\mu u_\mu)}{d\lambda} = -\frac{d\gamma}{d\lambda} = \frac{1}{3} \gamma^2 \theta + \frac{1}{2} \gamma^2 \Sigma (3n_r^2 - 1). \quad (\text{A.10})$$

To extract the remaining components, we can first expand the geodesic equation using Eqs. (A.6), (A.3), and (A.10) to obtain

$$\frac{dn^\mu}{d\lambda} = \frac{1}{3} \gamma \theta u^\mu - \gamma \sigma^\mu{}_\nu n^\nu + \frac{1}{2} \gamma \Sigma (3n_r^2 - 1) (u^\mu + n^\mu). \quad (\text{A.11})$$

Then we can write the radial component as

$$\frac{d(v^\mu r_\mu)}{d\lambda} = \frac{d(\gamma n^\mu r_\mu)}{d\lambda} \quad (\text{A.12})$$

$$= \frac{d\gamma}{d\lambda} n_r + \gamma \frac{dn^\mu}{d\lambda} r_\mu + \gamma n^\mu \frac{dr_\mu}{d\lambda}. \quad (\text{A.13})$$

The third term on the right-hand side of Eq. (A.13) can be evaluated as follows:

$$n^\mu \frac{dr_\mu}{d\lambda} = \gamma n^\mu r_{\mu;\nu} (u^\nu + n^\nu) \quad (\text{A.14})$$

$$= \gamma n_\theta \theta^\mu r_{\mu;\nu} n_\theta \theta^\nu \quad (\text{A.15})$$

$$= \gamma n_\theta^2 \theta^\mu \theta^\nu D_\nu r_\mu \quad (\text{A.16})$$

$$= \frac{1}{2} \gamma n_\theta^2 \theta_s. \quad (\text{A.17})$$

Here expression (A.15) follows from the normalization of r^μ and n^μ , spherical symmetry, and Eq. (A.3). Expression (A.17) uses the normalization of n^μ and the definition

$$\theta_s = D_\mu r^\mu \quad (\text{A.18})$$

for the ‘‘sheet expansion’’ θ_s , which measures the spatial rate of expansion of the spatial congruence r^μ on each comoving time slice. Combining Eqs. (A.10), (A.11), and (A.17), we finally obtain the radial component of the geodesic equation:

$$\frac{d(v^\mu r_\mu)}{d\lambda} = -\gamma^2 n_r H_\parallel + \frac{1}{2} \gamma^2 \theta_s n_\theta^2. \quad (\text{A.19})$$

We can obtain the final θ^μ component of the geodesic equation in a completely analogous manner to the radial component. However, we can do this more easily by taking the derivative with respect to λ of the identity

$$\gamma^2 = \gamma^2 n_r^2 + \gamma^2 n_\theta^2 = (v^\mu r_\mu)^2 + (v^\mu \theta_\mu)^2. \quad (\text{A.20})$$

After substituting Eqs. (A.10) and (A.19), the result is

$$\frac{d(v^\mu \theta_\mu)}{d\lambda} = -\gamma^2 n_\theta H_\perp - \frac{1}{2} \gamma^2 \theta_s n_r n_\theta. \quad (\text{A.21})$$

We now have all components of the null geodesic equation in covariant 1 + 1 + 2 notation. Our final step will be to express these equations in terms of coordinates along a null ray. The most natural choice of coordinates is the comoving, proper time coordinates implied by the LTB metric, Eq. (1). The single nontrivial angular coordinate will be taken to be the standard spherical coordinate θ

(ϕ will be constant). The link between the covariant geodesic equation and the coordinates x^μ is through the relation $v^\mu = dx^\mu/d\lambda$. In component form, we have

$$v^\mu u_\mu = -\frac{dt}{d\lambda}, \quad (\text{A.22})$$

$$v^\mu r_\mu = \frac{Y'}{\sqrt{1-K}} \frac{dr}{d\lambda}, \quad (\text{A.23})$$

$$v^\mu \theta_\mu = Y \frac{d\theta}{d\lambda}. \quad (\text{A.24})$$

Inserting Eqs. (A.22) to (A.24) into the geodesic equation components, Eqs. (A.10), (A.19), and (A.21), we finally obtain the coupled set of ordinary differential equations

$$\frac{dt}{d\lambda} = \gamma, \quad (\text{A.25})$$

$$\frac{dr}{d\lambda} = \gamma n_r \frac{\sqrt{1-K}}{Y'}, \quad (\text{A.26})$$

$$\frac{d\theta}{d\lambda} = \frac{\pm \gamma \sqrt{1-n_r^2}}{Y}, \quad (\text{A.27})$$

$$\frac{d^2 t}{d\lambda^2} = -\gamma^2 \left(H_\perp + \frac{3}{2} n_r^2 \Sigma \right), \quad (\text{A.28})$$

$$\begin{aligned} \frac{d^2 r}{d\lambda^2} = & - \left(\frac{dr}{d\lambda} \right)^2 \left(\frac{Y''}{Y'} + \frac{K'}{2(1-K)} \right) \\ & - 2\gamma \frac{dr}{d\lambda} H_\parallel + \left(\frac{d\theta}{d\lambda} \right)^2 \frac{Y(1-K)}{Y'}, \end{aligned} \quad (\text{A.29})$$

$$0 = \frac{d}{d\lambda} \left(Y^2 \frac{d\theta}{d\lambda} \right), \quad (\text{A.30})$$

$$\frac{dn_r}{d\lambda} = \frac{1}{2} \gamma (n_r^2 - 1) \left(3\Sigma n_r - \frac{2\sqrt{1-K}}{Y} \right). \quad (\text{A.31})$$

Here the expression $\theta_s = 2\sqrt{1-K}/Y$ has been used. Equation (A.30) represents the conservation of angular momentum. It is straightforward to verify that these equations are equivalent to those derived by more familiar techniques (e.g., [50]). The set (A.25) to (A.31) is overdetermined, and experimentation revealed the subset (16) to (19) (specialized to the decaying mode case of $K(r) = 0$) to be the most robust and numerically efficient.

[1] C. Blake et al., Mon. Not. Roy. Astron. Soc. **406**, 803 (2010), arXiv:1003.5721 [astro-ph.CO].
[2] K. Tomita, Astrophys. J. **529**, 38 (2000), arXiv:astro-ph/9906027.
[3] S. P. Goodwin, P. A. Thomas, A. J. Barber, J. Gribbin, and L. I. Onuora (1999), arXiv:astro-ph/9906187.
[4] M.-N. Celerier, Astron. Astrophys. **353**, 63 (2000), arXiv:astro-ph/9907206.
[5] J. W. Moffat and D. C. Tatarski, Astrophys. J. **453**, 17 (1995), arXiv:astro-ph/9407036.
[6] S. Foreman, A. Moss, J. P. Zibin, and D. Scott, Phys. Rev. **D82**, 103532 (2010), arXiv:1009.0273 [astro-

ph.CO].
[7] V. Marra and A. Notari, Class. Quant. Grav. **28**, 164004 (2011), arXiv:1102.1015 [astro-ph.CO].
[8] J.-P. Uzan, C. Clarkson, and G. F. R. Ellis, Phys. Rev. Lett. **100**, 191303 (2008), arXiv:0801.0068 [astro-ph].
[9] C. Clarkson, B. Bassett, and T. H.-C. Lu, Phys. Rev. Lett. **101**, 011301 (2008), arXiv:0712.3457 [astro-ph].
[10] J. P. Zibin, A. Moss, and D. Scott, Phys. Rev. Lett. **101**, 251303 (2008), arXiv:0809.3761 [astro-ph].
[11] A. Moss, J. P. Zibin, and D. Scott, Phys. Rev. **D83**, 103515 (2011), arXiv:1007.3725 [astro-ph.CO].
[12] T. Biswas, A. Notari, and W. Valkenburg, JCAP **1011**,

- 030 (2010), arXiv:1007.3065 [astro-ph.CO].
- [13] V. Marra and M. Paakkonen, JCAP **1012**, 021 (2010), arXiv:1009.4193 [astro-ph.CO].
- [14] P. Bull, T. Clifton, and P. G. Ferreira (2011), arXiv:1108.2222 [astro-ph.CO].
- [15] C. Clarkson and M. Regis, JCAP **1102**, 013 (2011), arXiv:1007.3443 [astro-ph.CO].
- [16] S. Nadathur and S. Sarkar, Phys. Rev. **D83**, 063506 (2011), arXiv:1012.3460 [astro-ph.CO].
- [17] R. A. Sunyaev and Y. B. Zeldovich, Mon. Not. Roy. Astron. Soc. **190**, 413 (1980).
- [18] J. Goodman, Phys. Rev. **D52**, 1821 (1995), arXiv:astro-ph/9506068.
- [19] J. Garcia-Bellido and T. Haugboelle, JCAP **0809**, 016 (2008), arXiv:0807.1326 [astro-ph].
- [20] C.-M. Yoo, K.-i. Nakai, and M. Sasaki, JCAP **1010**, 011 (2010), arXiv:1008.0469 [astro-ph.CO].
- [21] P. Zhang and A. Stebbins, Phys. Rev. Lett. **107**, 041301 (2011), arXiv:1009.3967 [astro-ph.CO].
- [22] J. P. Zibin and A. Moss, Class. Quant. Grav. **28**, 164005 (2011), arXiv:1105.0909 [astro-ph.CO].
- [23] G. Lemaitre, Ann. Soc. Sci. Bruxelles **53**, 51 (1933).
- [24] R. C. Tolman, Proc. Nat. Acad. Sci. **20**, 169 (1934).
- [25] H. Bondi, Mon. Not. Roy. Astron. Soc. **107**, 410 (1947).
- [26] R. R. Caldwell and A. Stebbins, Phys. Rev. Lett. **100**, 191302 (2008), arXiv:0711.3459 [astro-ph].
- [27] J. Silk, Astron. Astrophys. **59**, 53 (1977).
- [28] J. P. Zibin, Phys. Rev. **D78**, 043504 (2008), arXiv:0804.1787 [astro-ph].
- [29] L. Amendola and F. Finelli, Phys. Rev. Lett. **94**, 221303 (2005), arXiv:astro-ph/0411273.
- [30] M.-N. Celerier, K. Bolejko, and A. Krasinski, Astron. Astrophys. **518**, A21 (2010), arXiv:0906.0905 [astro-ph.CO].
- [31] T. Clifton, P. G. Ferreira, and J. Zuntz, JCAP **0907**, 029 (2009), arXiv:0902.1313 [astro-ph.CO].
- [32] I. D. Novikov, Sov. Astron. **8**, 857 (1965).
- [33] C. Hellaby and K. Lake, Astrophys. J. **290**, 381 (1985).
- [34] C. Hellaby and K. Lake, Astrophys. J. **282**, 1 (1984).
- [35] D. M. Eardley, Phys. Rev. Lett. **33**, 442 (1974).
- [36] E. W. Kolb and C. R. Lamb (2009), arXiv:0911.3852 [astro-ph.CO].
- [37] A. Stebbins (2007), arXiv:astro-ph/0703541.
- [38] D. J. Fixsen et al., Astrophys. J. **473**, 576 (1996), arXiv:astro-ph/9605054.
- [39] J. P. Zibin and D. Scott, Phys. Rev. **D78**, 123529 (2008), arXiv:0808.2047 [astro-ph].
- [40] V. F. Mukhanov, H. A. Feldman, and R. H. Brandenberger, Phys. Rept. **215**, 203 (1992).
- [41] R. K. Sachs and A. M. Wolfe, Astrophys. J. **147**, 73 (1967).
- [42] B. Paczynski and T. Piran, Astrophys. J. **364**, 341 (1990).
- [43] J. V. Arnao, M. J. Fullana, L. Monreal, and D. Saez, Astrophys. J. **402**, 359 (1993).
- [44] N. P. Humphreys, R. Maartens, and D. R. Matravers, Astrophys. J. **477**, 47 (1997), arXiv:astro-ph/9602033.
- [45] C. G. Tsagas, A. Challinor, and R. Maartens, Phys. Rept. **465**, 61 (2008), arXiv:0705.4397 [astro-ph].
- [46] G. F. R. Ellis and H. van Elst, NATO Adv. Study Inst. Ser. C. Math. Phys. Sci. **541**, 1 (1999), arXiv:gr-qc/9812046.
- [47] H. van Elst and G. F. R. Ellis, Class. Quant. Grav. **13**, 1099 (1996), arXiv:gr-qc/9510044.
- [48] C. A. Clarkson and R. K. Barrett, Class. Quant. Grav. **20**, 3855 (2003), arXiv:gr-qc/0209051.
- [49] C. Clarkson, Phys. Rev. **D76**, 104034 (2007), arXiv:0708.1398 [gr-qc].
- [50] H. Alnes and M. Amarzguioui, Phys. Rev. **D74**, 103520 (2006), arXiv:astro-ph/0607334.